*J. Fluid Mech.* (2007), *vol.* 586, *pp.* 147–176.  
doi:10.1017/S0022112007006878 Printed in the United Kingdom

# The contribution of shock tubes to simplified analysis of gas filtration through granular media

A. BRITAN, H. SHAPIRO AND G. BEN-DOR

Pearlstone Center for Aeronautical Engineering Studies, Protective Technologies R&D Center, Department of Mechanical Engineering, Faculty of Engineering Sciences, Ben-Gurion University of the Negev, Beer-Sheva, Israel

(Received 1 May 2006 and in revised form 1 April 2007)

A hybrid method for the problem of transient shock-induced filtration of the gas flow through granular media is developed. The hybrid method combines a controlled shock-tube test and Morrison's simplified approach to the problem of gas filtration. It is demonstrated that most pressure traces that have been recorded in various laboratories with a large variety of granular material samples and under different conditions are limited to situations in which the pressure losses in the flow are dominated by the Forchheimer mechanism. The hybrid method enables these results to be described by a single, universal pressure curve, and specification of the Forchheimer coefficient which is one of the two key parameters responsible for the correct simulation of the filtration-flow behaviour. The second key parameter, the Darcy coefficient, cannot be evaluated by the available experimental results. To overcome this shortcoming, a new controlled laboratory test that provides a wider range of the flow conditions, from the Forchheimer to the developed mixed flow, was conducted. In turn, a comprehensive gas dynamic analysis of the transient flow inside the shock tube enables us to define, from the single controlled laboratory test, the two coefficients of the Forchheimer resistance law, $a$ and $b$.

## 1. Introduction

### 1.1. *Formulation of the problem*

A situation in which a shock wave impacts a granular bed is observed quite often in soil mechanics. If a solid and heavy plate is placed at some distance underground, normal to the air/soil interface, the overpressure, $\Delta P_5$, applied at the air/soil interface is transformed inside the soil to a pulse of a diffusive type (Liang & Chao 1998). This pulse is usually characterized by a rise time, $t_R$, or the time required for the pressure to reach a specified percentage (usually 90 %) of its final equilibrium value, i.e. $\Delta P_5$ (Holman 1994). Owing to the scaling effects or other reasons, the peak pressures and the rise times registered in laboratory tests and those registered in free field tests can be different. The reasons for this difference could be evaluated by the computer modelling that is increasingly used nowadays (see e.g. Levy, Ben Dor & Sorek 1996; Sodre & Parise 1998; Sen *et al.* 2005). However, because computer modelling is still time consuming, experimental study that relies on empirical correlations predicting the transient and the spatial dynamics of the pressure pulse is a superior approach. Most investigators, when developing these correlations, limited themselves to easily obtainable and reliably measured parameters (e.g. granular sample length, porosity, etc.). The emphasis in these studies was on tests in shock tubes with short (about

several centimetres long) artificial granular samples of spherical particles (see e.g. Rogg, Hermann & Adomeit 1985; van der Grinten, van Dongen & van der Kogel 1985; Gelfand *et al.* 1989; Medvedev, Frolov & Gelfand 1990; Sakakita & Hayashi 1992; Engebretsen *et al.* 1996; Britan *et al.* 1997; Smeulders, van Dongen & Wisse 1997; Britan & Levy 2001; Mikami *et al.* 2001). In reality, however, when gas flows into a backfill following an explosion, granular layers that are orders of magnitude longer (a few metres) and contain non-spherical particles are of interest. Therefore, excluding the general principles or laws that could relate shock-tube data to real field conditions would make the pressure profiles that are recorded in shock-tube tests useless for general applications.

In this context the hybrid method, which is presented below, looks very promising since it allows the results of laboratory measurement to become closer to actual field conditions (see Britan *et al.* 2001*a*, 2006). The hybrid method combines a controlled shock tube test with Morrison's approach to the problem of gas filtration (Morrison 1972, 1976, 1977; Asay, Son & Bdzil 1996). In Morrison's approach the pressure gradient, $\partial P/\partial x$, in the filtration flow depends on the interstitial gas velocity $\tilde{V}$ in a generalized form that is commonly known as the *Forchheimer resistance law* (see also Lage 1998):

$$\frac{\partial P}{\partial x} = -a\tilde{\mu}\tilde{V} - b\tilde{\rho}\tilde{V}|\tilde{V}|. \tag{1.1}$$

The first term, the Darcy term $-a\tilde{\mu}\tilde{V}$, represents viscous losses, where $\tilde{\mu}$ is the gas viscosity (a tilde indicates dimensional values). The Darcy coefficient, $a$, is related to the commonly used granular layer permeability, $k_0$ and porosity, $\varepsilon$, through $a = \varepsilon/k_0$. The second term, the Forchheimer term $-b\tilde{\rho}\tilde{V}|\tilde{V}|$, where $\tilde{\rho}$ is the gas density and $b$ is the Forchheimer coefficient, models the bulk form-drag force effect that is frequently termed in the literature-inertial losses (Lage & Antohe 2000). The Darcy and the Forchheimer coefficients, $a$ and $b$, respectively, include reliably measured characteristics of granular media, and hence their exact values are the key parameters for correctly simulating the filtration flow.

For a granular medium composed of spherical granules, the Darcy, $a$, and the Forchheimer, $b$, coefficients are functions of only the particle diameter, $d_p$, and the granular medium porosity, $\varepsilon$, through the following relations (Ergun 1952 and Macdonalds *et al.* 1979):

$$a_0 = 180\frac{(1-\varepsilon)^2}{\varepsilon^2}\frac{1}{d_p^2}, \qquad b_0 = 1.8\frac{1-\varepsilon}{\varepsilon}\frac{1}{d_p}. \tag{1.2a, b}$$

The subscript 0 denotes that these coefficients are for a granular medium that is composed of spherical granules. Note that under these circumstances $a_0 = 55.55b_0^2$.

This study starts with a brief summary of a simplified mathematical model and several important consequences, which are readily apparent from the model and make the theoretical analysis more feasible. Then the strategy of the hybrid method is presented. Conceptually, it is identical to a numerical simulation of the results obtained in parallel with a controlled laboratory test. The prime objective of the physical test is recording the gas pressure traces along a granular sample that is placed against the rigid endwall of the shock tube and is subject to a normal impact by a shock wave of a known intensity. The resulting pressure traces enable one to specify the rise times, $t_R$, as a function of the granular sample properties. This in turn characterizes the dynamic response of the material to the impact. Further processing of these data provides the value of the Forchheimer coefficient, $b$. With this value in

hand the test is repeated with a much longer sample of the same material. Matching between the simulated and the recorded pressure traces finally results in the value of the Darcy coefficient, $a$. The reliability of the proposed method is illustrated by numerous examples of regular shock tube tests with a focus on the critical importance of the ratio of the rise time to the test time. As a last example, a recent shock tube test with a 2.5 m long granular sample composed of natural quartz sand is presented, analysed and discussed. A comprehensive analysis of the data obtained made it possible to specify both the Darcy, $a$, and the Forchheimer, $b$, coefficients.

### 1.2. *Governing equations*

Prior to presenting the basic equations for the pressure rise that were developed by Morrison (1972, 1976, 1977) the two non-dimensional parameters that were introduced by Morrison (1972) to specify the type of filtration flow inside a granular column of length, $l$, are introduced:

$$N = \frac{P_5 - P_1}{P_1} = \frac{\Delta P_5}{P_1}, \tag{1.3a}$$

$$Re_f = \frac{\tilde{\rho}_1 \Delta P_5}{\tilde{\mu}_1^2} \frac{b}{a^2} \frac{1}{l} = \frac{b}{a^2} \frac{1}{l} \frac{N \tilde{c}_1^2}{\tilde{\nu}_1^2 \gamma}. \tag{1.3b}$$

Here $N$ is the non-dimensional intensity of the pressure impact that is imposed by the shock wave reflected at the front edge of the granular sample, i.e. at its entrance, $Re_f$ is the effective Reynolds number, $\tilde{\nu}_1$ is the kinematic viscosity, $\tilde{\rho}_1$ is the density (note that $\tilde{\nu}_1 = \tilde{\mu}_1/\tilde{\rho}_1$ where $\tilde{\mu}_1$ is the dynamic viscosity) and $\tilde{c}_1$ is the sound velocity (i.e. $\tilde{c}_1^2 = (\gamma P_1)/\tilde{\rho}_1$) (subscript 1 refers to the parameters of the quiescent air ahead of the incident shock wave). Note that this Reynolds number, which was originally introduced by Morrison (1977), includes the granular column length, $l$, and the parameters $a$ and $b$ which are closely related to the permeability and porosity of the granular medium which, in turn, is related to the characteristic pore length. Hence, the Reynolds number implicitly includes the pore length scale.

For reasons of convenience, the phenomenon will be analysed using a non-dimensional approach. Since in Morrison's approach the gas flow through the granular column was considered to be isothermal, the density $\tilde{\rho}$ can expressed as $\tilde{\rho} = \tilde{\rho}_1(1 + N\theta)$, where $\theta = (P - P_1)/\Delta P_5$ is the non-dimensional pressure. All the information on the specific parameters of the granular medium, e.g. porosity, particle diameter or shape, is included in the Darcy and the Forchheimer coefficients. The non-dimensional variables for the distance, $x$, and the time, $t$, are

$$\chi = \frac{x}{l}, \qquad \tau_1 = \frac{t}{t_{sc1}}, \tag{1.4a, b}$$

where $l$ is the length of the granular column and $t_{sc1} = l/V_{sc}$. Following Morrison (1972) the scaling factor for the velocity is $V_{sc} = (\Delta P_5)/(al\tilde{\mu}_1)$. Thus the scaling factor for the time, $t_{sc1}$, is

$$t_{sc1} = l^2 \frac{\gamma \tilde{\nu}_1}{\tilde{c}_1^2 N} a. \tag{1.4c}$$

As a consequence the non-dimensional form of the Forchheimer resistance law (equation (1.1)) is

$$\frac{\partial \theta}{\partial \chi} = -V - Re_f (1 + N\theta) V |V|. \tag{1.5a}$$

The mass conservation equation becomes

$$N\frac{\partial\theta}{\partial\tau_1}+\frac{\partial}{\partial\chi}\left[V\left(1+N\theta\right)\right]=0. \tag{1.5b}$$

Combining equations (1.5*a*) and (1.5*b*) results in

$$\frac{\partial\theta}{\partial\tau_1}=\frac{1}{\sqrt{1+4Re_f(1+N\theta)\left|\dfrac{\partial\theta}{\partial\chi}\right|}}\left[\left(\frac{1}{N}+\theta\right)\frac{\partial^2\theta}{\partial\chi^2}+\left(\frac{\partial\theta}{\partial\chi}\right)^2\right]. \tag{1.6}$$

Equation (1.6), in which both the viscous and the inertial losses are accounted for, describes the non-dimensional pressure distribution along the granular column. In fact, it describes filtration flows that comply with the so-called *mixed-flow conditions*, i.e. flows in which both the viscous and the inertial losses are dominant.

When $Re_f>1$ it is more convenient to replace, in equation (1.6), the time scaling parameter, $\tau_1$, by another time scaling parameter, $\tau_2$ (see Morrison 1976):

$$\tau_2=\frac{t}{t_{sc2}}, \tag{1.7a}$$

where

$$t_{sc2}=t_{sc1}\sqrt{Re_f}=\frac{l^{1.5}}{\tilde{c}_1}\sqrt{\frac{b\gamma}{N}}. \tag{1.7b}$$

With $t_{sc2}$ in hand equation (1.6) assumes a form which also describes filtration flows that comply with the so-called mixed-flow conditions, when the role of the viscous losses is much smaller:

$$\frac{\partial\theta}{\partial\tau_2}=\sqrt{\frac{Re_f}{1+4Re_f\left(1+N\theta\right)\left|\partial\theta/\partial\chi\right|}}\left[\left(\frac{1}{N}+\theta\right)\frac{\partial^2\theta}{\partial\chi^2}+\left(\frac{\partial\theta}{\partial\chi}\right)^2\right]. \tag{1.8}$$

When only viscous losses dominate, i.e. when $Re_f\to 0$, equation (1.6) is reduced to

$$\frac{\partial\theta}{\partial\tau_1}=\left(\frac{1}{N}+\theta\right)\frac{\partial^2\theta}{\partial\chi^2}+\left(\frac{\partial\theta}{\partial\chi}\right)^2, \tag{1.9a}$$

which describes filtration flows that comply with the so-called *Darcy-flow conditions* or the *Darcy-flow domain*. Note that while the Darcy flow is by definition linear, substitution of the gas velocity $V=-\partial\theta/\partial\chi$ into the mass conservation equation (1.5*b*) results in nonlinear equation (1.9*a*). When only inertial losses dominate, i.e. when $Re_f\to\infty$, the common equation (1.8) is reduced to

$$\frac{\partial\theta}{\partial\tau_2}=\frac{0.5}{\sqrt{\left(1+N\theta\right)\left|\partial\theta/\partial\chi\right|}}\left[\left(\frac{1}{N}+\theta\right)\frac{\partial^2\theta}{\partial\chi^2}+\left(\frac{\partial\theta}{\partial\chi}\right)^2\right], \tag{1.9b}$$

which describes filtration flows that comply with the so-called *Forchheimer-flow conditions* or the *Forchheimer-flow domain*.

The problem of numerically simulating gas filtration could be formulated as follows. A granular sample of unit length is subject to a pressure step loading at its front edge while at its rear end an impermeability condition is imposed. The objective is to calculate the non-dimensional pressure distribution along the sample length. Note that neither equation (1.9*a*) nor (1.9*b*) includes specific parameters of the granular medium considered. Hence their solutions are valid for granular samples of any length and

properties. Unlike (1.9), equations (1.6) and (1.8) depend directly or explicitly (recall that $\tau = f(a)$] on the material properties through the effective Reynolds number, $Re_f$. The boundary conditions, which are the same for all the above-mentioned forms of Morrison's equations (equations (1.6), (1.8), (1.9*a*) and (1.9*b*) are

$$\theta(0, \tau) = 1, \quad \partial\theta(1, \tau)/\partial\chi = 0, \tag{1.10a}$$

and the initial condition, which is also the same for all these equations, is

$$\theta(\chi, 0) = 0. \tag{1.10b}$$

### 1.3. *Similarity of the pressure profiles and the boundaries between the various flow domains*

Since the two extreme flow domains that are described by equations (1.9*a*) and (1.9*b*) include only a single parameter, $N$, their solutions, namely the non-dimensional pressure profile, $\theta(\tau)$, are invariant with the properties of the granular samples. This feature of universality has some important consequences:

(i) The first is the interchangeability of the pressure profiles. This feature is valid for two granular samples of different lengths, but composed of the same material and subjected to a similar and constant pressure loading that complies with the boundary conditions (1.10*a*). This means that the dimensional pressure profile, $P(x_l, t)$, recorded in the cross-section $x_l$ of a granular sample of length $l$, is identical to the scaled pressure profile, $P(x_L, t^*)$, recorded in the cross-section $x_L$ of another granular sample that is composed of the same material but has a different length $L$, provided

$$x_L = x_l(L/l) \quad \text{and} \quad t^* = t(L/l)^j, \tag{1.11}$$

where $j = 2$ for the Darcy flow and $j = 1.5$ for the Forchheimer flow. (Note that the difference in the power $j$ arises from equations (1.4*c*) and (1.7*b*).

(ii) The second is related to the non-dimensional rise times, $\tau_1^D$ and $\tau_2^F$. Based on the non-dimensional notation, the rise time implies that $\theta(\chi, \tau)|_{\chi=1} = 0.9$. For the known impact intensity, $N$, the rise times $\tau_1^D$ and $\tau_2^F$ are universal constants that show no dependence on the material properties. Then equations (1.4*b*) and (1.4*c*) imply that in the Darcy-flow domain:

$$t_R^D = l^2 \left( \frac{\gamma \tilde{\nu}_1}{\tilde{c}_1^2 N} a \right) \tau_1^D. \tag{1.12}$$

Similarly, equations (1.7*a*) and (1.7*b*) imply that in the Forchheimer-flow domain:

$$t_R^F = l^{1.5} \left( \frac{1}{\tilde{c}_1} \sqrt{\frac{b\gamma}{N}} \right) \tau_2^F. \tag{1.13}$$

As will be shown below, the concept of the two limiting flow domains is the main tool for both the data processing and the scaling of the pressure traces that are obtained in controlled laboratory tests to real field conditions.

The present discussion centres on the techniques that specify the domains appropriate to the different flow types. The manner in which the boundaries separating the limiting flow domains were determined is demonstrated in figures 1(*a*) and 1(*b*). Using a fixed value of $N$ and continuously varying the Reynolds number, $Re_f$, numerical solutions of equation (1.6) were generated until the resulting endwall pressure curve matched one of the limiting curves that are described by either equation (1.9*a*) or equation (1.9*b*). Since the resulting rise time, $\tau_R$, also tends to the limiting values $\tau_1^D$ or $\tau_2^F$, the final decision on the optimal matching was based on a

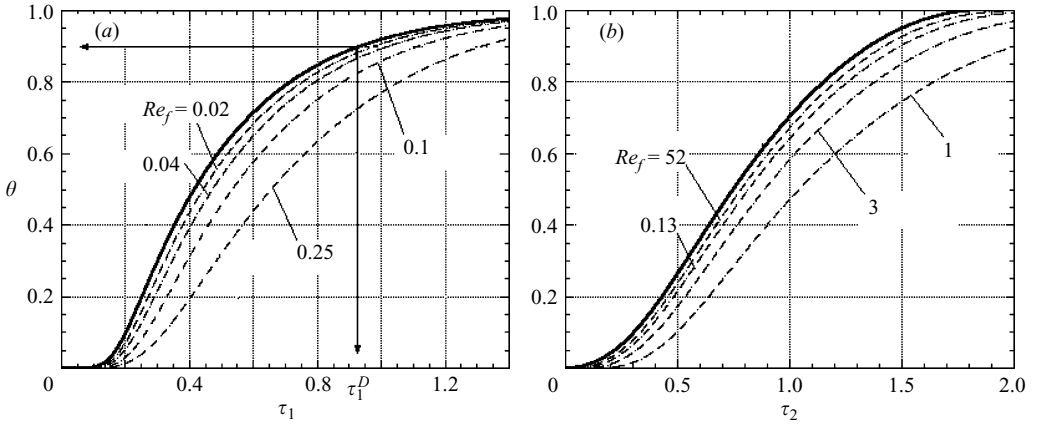


FIGURE 1. Two typical examples demonstrating the method that specifies the critical values of the Reynolds number, $Re_f$, for (*a*) Darcy and (*b*) Forchheimer flows. The incident shock wave Mach number is $M_s = 1.4$. The limiting curves are shown by thick solid lines. The thin solid lines with arrows show the rise time for the limiting curve.

comparison between these values. The simulated pressure profiles were considered to be equivalent of the limiting curves if the relative differences between the rise times, $\tau_R$ and $\tau_1^D$ or $\tau_2^F$, was less than 7 %, i.e.

$$\Delta\tau_1 = \frac{\tau_r - \tau_1^D}{\tau_1^D} \leqslant \Delta = 0.07, \qquad \Delta\tau_2 = \frac{\tau_r - \tau_2^F}{\tau_2^F} \leqslant \Delta = 0.07 \tag{1.14a, b}$$

The Reynolds number that ensures optimal matching can be referred to as a 'critical' Reynolds number for the Darcy, $Re_f^D$, or for the Forchheimer, $Re_f^F$, flow domains. Note that $\Delta = 7\,\%$ is large enough to distinguish between the two pressure curves. This value is usually adopted as the standard uncertainty of pressure measurements in shock tube tests.

After obtaining a series of solutions for shock-wave Mach numbers in the range $1.1 \leqslant M_s \leqslant 2.0$, the following two correlations describing the boundary separating the three flow domains mentioned above were specified:

(i) The boundary separating the Darcy- and the mixed-flow domains is

$$Re_f^D = 0.1188 M_s^{-3.448}. \tag{1.15}$$

(ii) The boundary separating the mixed- and the Forchheimer-flow domains is

$$Re_f^F = 85.458 M_s^{-4.181}. \tag{1.16}$$

Hence:

(i) Experiments for which $Re_f < Re_f^D$ comply with the Darcy-flow domain,

(ii) experiments for which $Re_f > Re_f^F$ comply with the Forchheimer-flow domain, and

(iii) experiments for which $Re_f^D < Re_f < Re_f^F$ comply with the mixed-flow domain.

The corresponding two correlations for the non-dimensional rise times are

$$\tau_1^D = -14.184 + 31.932 M_s - 25.693 M_s^2 + 9.249 M_s^3 - 1.251 M_s^4, \tag{1.17}$$

$$\tau_2^F = -3.206 + 3.255 M_s. \tag{1.18}$$

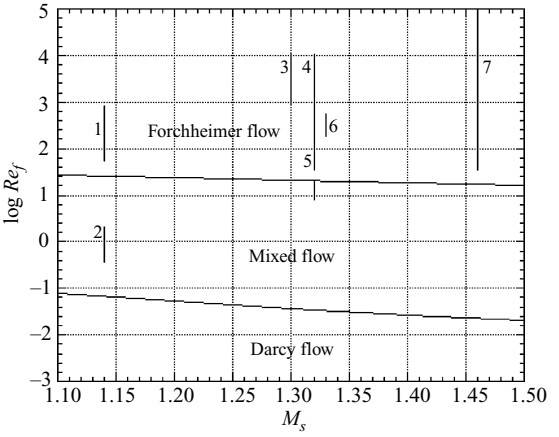


FIGURE 2. The initial conditions of relevant experiments conducted in conventional shock tube in a variety of laboratories. The vertical lines indicate the experiments that are detailed in table 1. The numbers correspond to the Test no. column in table 1.

## 2. Strategy for the controlled laboratory test

The main objective of the hybrid method developed here which specifies the values of the Darcy coefficient, $a$, and the Forchheimer coefficient, $b$, in the so-called *Forchheimer resistance law* (see equation (1.1)), is to record the transient pressure field upstream and inside the granular column. Measurements of this kind have been the subject of many published experimental investigations; the range of the conditions that were involved in these experiments has not been analysed yet. As will be shown below, this range has a particular importance because it determines how far the problem could be solved in conventional laboratory tests.

### 2.1. *Shock tube capabilities*

Figure 2 presents the conditions of 42 different shock-tube experiments (by others and ours) that have been published over the years in the literature (for details see table 1). Since most of the granular samples in these experiments were artificial and were composed of smooth spherical granules, the effective Reynolds numbers were calculated from

$$Re_f = \left(\frac{\varepsilon}{1-\varepsilon}\right)^3 \frac{1}{18000}\frac{N}{\tilde{v}_1^2}\frac{d_p^3}{l}\frac{\tilde{c}_1^2}{\gamma}, \tag{2.1}$$

which is readily obtained from equations (1.2$a$), (1.2$b$) and (1.3$b$). Figure 2 reveals that:

1. All but two sets of experimental results fall in the Forchheimer-flow domain.
2. There are very few experimental results in the mixed-flow domain. These are the experiments with the smallest particles $d_p \leqslant 0.5$ mm and the relatively long granular samples $l \geqslant 80$ mm or experiments with short samples that are composed of sandstone-like porous material.
3. There are no experiments in the Darcy-flow domain.
4. For the considered range of incident shock wave Mach numbers, $1.1 \leqslant M_s \leqslant 1.5$, the lowest value of the effective Reynolds number was obtained in the experiments of van der Grinten *et al.* (1985). However even for this case, the relatively long granular column composed of natural sand that was used was not sufficient to be in the Darcy-flow domain.

| Test no. | $M_s$ | Material | $l$ [mm] | $d_p$ [mm] | $\varepsilon$ | $Re_f$ | Source |
|---|---|---|---|---|---|---|---|
| 1.1–1.2 | 1.14 | Glass | 56; 61 | 3.0; 1.3 | 0.32 | 772; 57 | Smeulders *et al.* (1997) |
| 2.1 | 1.14 | Sand | 152.5 | 0.5 | 0.35 | 1.97 | ” |
| 2.2 | 1.14 | Sand | 1895 | 0.5 | 0.33 | 0.121 | van der Grinten *et al.* (1985) |
| 3.1–3.3 | 1.32 | $Al_2O_3$ | 22.5–138 | 1.67 | 0.46 | 924–5670 | Britan *et al.* (1997) |
| 3.4–3.7 | 1.32 | PVC | 39-138 | 3.33 | 0.39 | 3094–10964 | ” |
| 4.1–4.8 | 1.32 | Steel | 17–138 | 1.04 | 0.40 | 107–867 | ” |
| 4.9–4.12 | 1.32 | Potash | 12–53 | 0.45 | 0.43 | 33–144 | ” |
| 5 | 1.32 | Steel | 81, 138 | 0.45 | 0.39 | 7.6–13 | ” |
| 5 | 1.32 | Potash | 96; 138 | 0.45 | 0.43 | 12.6–17.7 | ” |
| 6 | 1.33 | Ceramic | 15–60 | 0.77 | 0.44 | 171–683 | Mikami *et al.* (2001) |
| 7.1–7.7 | 1.46 | Steel | 5–60 | 0.5 | 0.4 | 46–555 | Britan *et al.* (2001*b*) |
| 7.8–7.11 | 1.46 | Glass | 5–38 | 0.5 | 0.4 | 73–555 | ” |
| 7.12–7.15 | 1.46 | Rimax | 30–66 | 1.0 | 0.35 | 177–390 | ” |
| 7.16–7.18 | 1.46 | Rimax | 48–84 | 2.4 | 0.42 | 4682–8195 | ” |
| 7.19 | 1.46 | Steel | 22 | 4.4 | 0.49 | 257,340 | ” |
| 7.20–7.22 | 1.46 | Steel | 12–63 | 2.0 | 0.39 | 2487–13056 | ” |
| 7.23–7.25 | 1.46 | Steel | 4–49 | 1.0 | 0.35 | 238–2924 | ” |
| 8 | 1.31 | Sand-Stone | 20 | | 0.23 | 2.85 | Smeulders *et al.* (1997) |

TABLE 1. Conditions of 42 published experiments that were conducted in different shock tubes.

This situation is a direct result of the fact that the shock-tube length restricts the duration (i.e. the test time, $\Delta t_5$) of steady conditions at the entrance cross-section (i.e. the front edge) of the granular column. For reliable measurements, the rise time, $t_R$, has to be at most equal to $\Delta t_5$, i.e.

$$t_R \leqslant \Delta t_5. \tag{2.2}$$

Based on the ‘classical’ shock-tube theory (see e.g. Nishida 2001) the test time, $\Delta t_5$, for weak shock waves ($M_s < 2$) is

$$\Delta t_5 \approx \frac{\tilde{\rho}_1}{\tilde{\rho}_2}\frac{l_{ch}}{\tilde{c}_1 M_s}. \tag{2.3}$$

Here $l_{ch}$ is the length of the shock-tube channel (driven section),

$$\frac{\tilde{\rho}_2}{\tilde{\rho}_1} = \frac{(\gamma+1)\,M_s^2}{2+(\gamma-1)M_s^2}$$

is the density ratio across the incident shock wave, $\tilde{c}_1$ is the speed of sound in undisturbed air, and $\gamma = 1.4$ is the adiabatic coefficient. Replacing $\tilde{\rho}_2/\tilde{\rho}_1$ in equation (2.3) results in

$$\Delta t_5 \approx \frac{l_{ch}\left[2+(\gamma-1)M_s^2\right]}{(\gamma+1)\tilde{c}_1 M_s^3}. \tag{2.4}$$

For spherical particles, inside the Forchheimer-flow domain, the dimensional rise time, $t_R$, could be obtained using correlation (1.18), where the parameter $\tau_2^F$ is equal to $t_R/t_{sc2}$. Here $t_{sc2}$ is the time-scaling parameter, which was introduced in (1.7*b*), and the Forchheimer coefficient, $b$, is given by equation (1.2*b*). The resulting expression for the dimensional rise time, $t_R$, is

$$t_R = \tau_2^F t_{sc2} = \tau_2^F l\sqrt{1.8\frac{l}{d_p}\frac{\tilde{\rho}_1}{\tilde{\rho}_2}\frac{\gamma P_1}{\Delta P_5}\frac{1-\varepsilon}{\varepsilon}}. \tag{2.5}$$

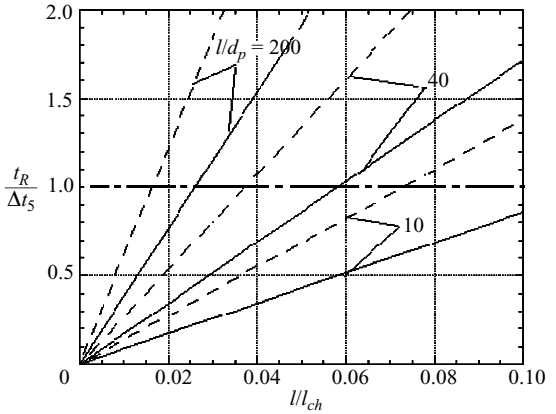


FIGURE 3. Results of a series of solutions of equation (2.6) for two values of the incident shock-wave Mach number $M_s = 1.3$ (solid lines) and $M_s = 1.5$ (dashed lines) and three relative lengths of the granular sample $l/d_p = 10$, 40 and 200.

In order to clarify the conditions when the requirement (2.2) is met one has to calculate the ratio of the rise time, $t_R$, to the duration of the shock-tube test time, $\Delta t_5$, for typical shock-tube test parameters. Using equations (2.4) and (2.5) one obtains

$$\frac{t_R}{\Delta t_5} = \tau_2^F \frac{l}{l_{ch}} \sqrt{1.8 \frac{l}{d_p} \frac{1-\varepsilon}{\varepsilon} \frac{\gamma+1}{2\left(M_s^2-1\right)}} \frac{M_s^2(\gamma+1)}{2+(\gamma-1)M_s^2}. \tag{2.6}$$

A series of solutions of equation (2.6) for two typical values of incident shock-wave Mach number, $M_s = 1.3$ and $M_s = 1.5$, and three relative lengths of the granular sample, $l/d_p = 10$, 40 and 200, yield the data shown in figure 3. The horizontal line corresponds to the condition $t_R = \Delta t_5$. The domain under this line provides the conditions for reliable measurements of $t_R$. Figure 3 reveals that:

(i) By comparing the calculated straight lines, it is clear that the parameter $t_R/\Delta t_5$ increases when $l/d_p$ or $l/l_{ch}$ increases. Thus, increases in $l$ or decreases in $d_p$ result in an increase in $t_R$. This supports our earlier conclusion that experiments in a standard shock tube with small particles or long granular columns are restricted by the duration of the test time, $\Delta t_5$.

(ii) An additional way of testing long granular columns could be to change the shock wave Mach number $M_s$: when it decreases, the granular sample length could be increased (compare the dashed and solid lines).

To demonstrate the role of the small particles in the rise time, $t_R$, refer to the results of test number 2.2 of table 1 shown in figure 4. While the step-like input pressure, $P_5$, remains steady during a rather long time period of about $\Delta t_5 \approx 10$ ms, the pressure traces indicate that equilibrium was not reached even at the pressure port that was nearest to the entrance of the granular sample ($x = 20$ mm). This was due to the small size of the sand particles ($d_p = 0.3$ mm) that resulted in a very small permeability of the granular column. It is clear that any attempt to specify the rise time, $t_R$, far downstream from the entrance of the granular column in this test is doomed to fail. In support of this conjecture equation (2.6) was solved for a test time duration of $\Delta t_5 = 3$ ms and two limiting values of the particle's diameter, $d_p$. The resulting curves, $l = F(M_s)$, shown in figure 5, clearly indicate that the lengths of the granular samples, $l$, which provide a means for evaluating the rise time, $t_R$, have to be within the narrow

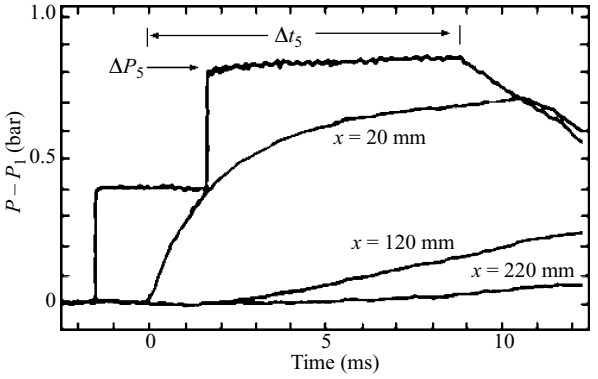


FIGURE 4. Pressure signals registered upstream of and inside (at $x = 20$ mm, 120 mm, and 220 mm) a granular column 1.895 m long (van der Grinten *et al.* 1985).

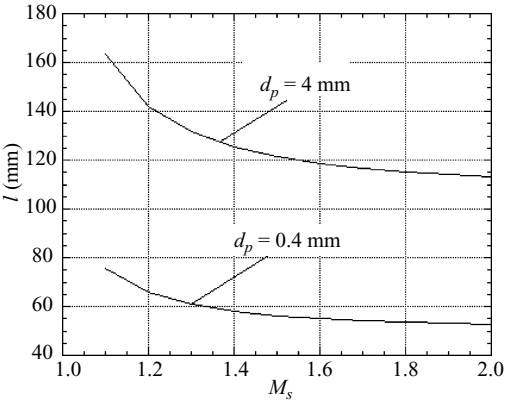


FIGURE 5. Calculated length of the granular sample vs. Mach number for a test time duration of $\Delta t_5 = 3$ ms and two limiting values of the diameter of the particle.

domain of about 60–150 mm. As expected, a similar conclusion is evident from the results shown in table 1 where it can be seen that all but two of the tested samples (2.1 and 2.2) have a length $l \leqslant 150$ mm.

### 2.2. *Data processing*

Since regular shock tubes are best suited for producing Forchheimer-flow conditions the resulting pressure traces could be used to specify the Forchheimer coefficient, $b$.

*Evaluation of the Forchheimer coefficient, b*

The procedure for evaluating the Forchheimer coefficient, $b$, in a controlled laboratory test, is split into four distinct steps:

1) A set of probing granular samples of various lengths $l < 200$ mm is tested for which it is likely that, at the end of the sample, the flow still complies with the Forchheimer domain. The tested conditions should be similar (i.e. the same granular material, ambient temperature and impact intensity).

2) The rise times, $t_R$, are deduced from the recorded pressure traces.

3) The assumption that the resulting flow fields correspond to the Forchheimer-flow domain must be confirmed. Based on equation (1.13), when this indeed is the

case, the ratio of the measured rise times to $l^{1.5}$ should not depend on the sample length, since

$$\frac{t_R^F}{l^{1.5}} = \left(\frac{1}{\tilde{c}_1}\sqrt{\frac{b\gamma}{N}}\right)\tau_2^F = K^F = \text{Const.} \tag{2.7}$$

If this indeed is the case, the Forchheimer coefficient, $b$, could be readily obtained from

$$b = \left[\frac{\tilde{c}_1 K^F}{\tau_2^F(M_s)}\right]^2 \frac{N}{\gamma}. \tag{2.8}$$

*Evaluation of the Darcy coefficient, a*

Adopting the above idea to evaluate the Darcy coefficient, $a$, suggests that one should perform a set of controlled laboratory tests with much longer granular samples in order to obtain a new set of rise times that correspond to the Darcy-flow domain ($Re_f < Re_f^D \approx 0.1$). Similarly to the foregoing presentation and based on equation (1.12), this could be verified by checking whether the requirement

$$\frac{t_R^D}{l^2} = \left(\frac{\gamma\tilde{\nu}_1}{\tilde{c}_1^2 N}a\right)\tau_1^D = K^D = \text{Const.} \tag{2.9}$$

is fulfilled. If this is the case, then the Darcy coefficient, $a$, could be calculated from

$$a = \frac{\tilde{c}_1^2 K^D}{\tau_1^D(M_s)}\frac{N}{\tilde{\nu}_1\gamma}. \tag{2.10}$$

Recall that correlation (1.17) for the non-dimensional rise time, $\tau_1^D$, was specified using the procedure demonstrated in figure 1(*a*). Since the critical values of $Re_f < Re_f^D$ and $\tau_1^D$ were specified using the series of calculations of the endwall pressure profiles, this ensures that the Darcy regime dominates, at least near the endwall. At the same time, the upstream flow, which is much closer to the granular sample entrance, could comply with the mixed or even Forchheimer flow conditions.

Unfortunately, our estimates, which are detailed in § 2.1, clearly show that the related value of $Re_f^D$ must be extremely small for this case ($Re_f^D \leqslant 0.1$). In fact, a standard experimental design that is based on the endwall measurement and meets the requirement $Re_f^D \leqslant 0.1$ requires a granular sample of several metres long. A similar consideration for the sidewall measurements (post-transmitted shock-wave filtration flow) requires a sample that is tens of metres long. Since in experiments with extremely long granular samples the rise times could reach tens of seconds such shock tube tests are impractical for evaluating the Darcy coefficient $a$. Alternatively, the problem could be solved by performing controlled laboratory tests in the mixed-flow domain, i.e. $10 \approx Re_f^F > Re_f > Re_f^D \approx 0.1$ (see figure 2). The controlled laboratory tests again start with short granular samples that ensure Forchheimer-flow conditions from which the Forchheimer coefficient, $b$, could be found using the procedure described above. Then, the resulting value of $b$ is used as an input to generate the numerical solutions of the common equation (1.8) with various values of $a$. Optimal matching of the predicted and measured pressure curves provides the best value of $a$.

Unfortunately, the required length of the granular sample in order to be in the mixed-flow domain is still too long. As a result, during a major part of the recording period, in most shock tubes of regular size, the input conditions become unsteady. Hence the numerical solution of the common equation (1.8) for this case must be

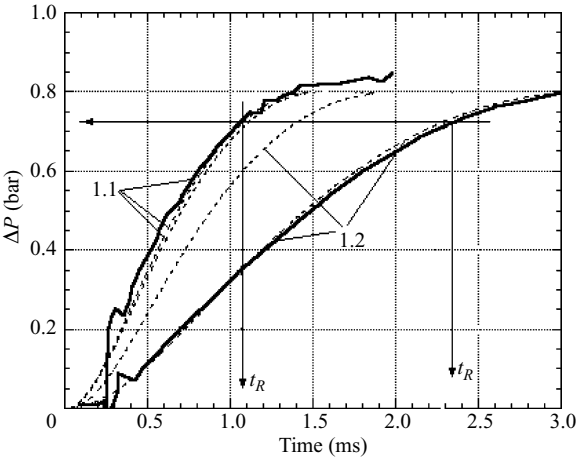


FIGURE 6. Comparison between the measured (solid lines) and simulated (dashed and dotted lines) endwall pressure signals. The experiments were reported by Smeulders *et al.* (1997). The numbers of the experiments refer to table 1. Experiment 1.1: $d_p = 3$ mm and $l = 56$ mm; Experiment 1.2: $d_p = 1.3$ mm and $l = 61$ mm.

performed using the actual boundary condition (pressure) that is acting at the front edge of the granular sample.

## 3. Validation and typical applications

The diversity of the granular materials distributed throughout the world might suggest that laboratory tests have little in common with real practical needs. Morrison's (1972, 1976, 1977) approach was the first attempt to overcome this by combining the data in a pattern suitable for practical use. However, due to the oversimplifications in his approach, the salient features that stemmed from it, namely similar solutions, limiting pressure profiles and the boundaries between the different filtration flow domains, require experimental verification. As will be shown below, results of shock-tube tests, which fall in the Forchheimer-flow domain, are of special interest for verification.

The first candidates for the validation procedure are the two pressure traces that are presented in figure 6 by thick solid lines. The distinctive feature of these tests is the significant difference between the diameters of the granules, $d_p$, of the samples, which were nearly similar in their lengths, $l$ (in test 1.1 $d_p = 3.0$ mm and $l = 56$ mm and in test 1.2 $d_p = 1.3$ mm and $l = 61$ mm. Using the porosity, $\varepsilon$, the Forchheimer coefficient, $b$, and the mean granule diameter, $d_p$, that were reported by the authors, the calculated Reynolds number, $Re_f$, revealed that the test conditions corresponded to the Forchheimer-flow domain. To ensure that this indeed was the case, the above-mentioned four-step procedure was performed. First the rise time, $t_R$, which by definition is the time corresponding to $0.9\Delta P_5$, was deduced from the pressure profile (see the thin solid lines in figure 6). Then, using correlation (2.5) and equation (2.8) the values of the Forchheimer coefficients, $b$, were calculated for each of these curves. The significant discrepancy between the results available in the literature is shown in table 2. For example, in test 1.2 the value of $b$ as obtained by our analysis was more than twice that predicted using Ergun's coefficient, $b_0$, which assumes spherical particles. In contrast, the coefficient $b$ reported for this material by Smeulders *et al.*

| Test no. | Material | $d_p$ [mm] | $l$ [mm] | $t_R$ [ms] | $K^F \times 10^3$ [ms/mm$^{1.5}$] | $b$ [$m^{-1}$] | $b_0$[$m^{-1}$] |
|---|---|---|---|---|---|---|---|
| 1.1 | Glass | 3 | 56 | 1.08 | 2.62 | 1675 [1741(1)] | 1275 |
| 1.2 | Glass | 1.3 | 61 | 2.28 | 4.79 | 6250 [2115(1)] | 3082 |
| 3.1 | $Al_2O_3$ | 1.67 | 22.5 | 0.35 | 3.28 | 1874 | 1125 |
| 3.2 | $Al_2O_3$ | 1.67 | 67 | 1.75 | 3.25 | 1844 | – |
| 3.3 | $Al_2O_3$ | 1.67 | 84 | 2.50 | 3.25 | 1836 | – |
| 3.4 | PVC | 3.33 | 39 | 0.58 | 2.24 | 870 | 845 |
| 3.5 | PVC | 3.33 | 58 | 1.00 | 2.26 | 890 | – |
| 3.6 | PVC | 3.33 | 95 | 2.10 | 2.26 | 890 | – |
| 3.7 | PVC | 3.33 | 138 | 3.60 | 2.22 | 858 | – |
| 4.1 | Steel | 1.04 | 17 | 0.28 | 3.99 | 2651 | 2596 |
| 4.2 | Steel | 1.04 | 32 | 0.72 | 3.97 | 2635 | – |
| 4.3 | Steel | 1.04 | 49 | 1.35 | 3.96 | 2572 | – |
| 4.4 | Steel | 1.04 | 69 | 2.24 | 3.91 | 2545 | – |
| 4.5 | Steel | 1.04 | 81 | 2.90 | 3.97 | 2635 | – |
| 4.6 | Steel | 0.45 | 26 | 0.82 | 6.16 | 6318 | 6254 |
| 4.7 | Steel | 0.45 | 35 | 1.28 | 6.18 | 6359 | – |
| 4.8 | Steel | 0.45 | 43 | 1.70 | 6.04 | 6074 | – |
| 4.9 | Potash | 0.45 | 12 | 0.38 | 8.89 | 13170 | 5300 |
| 4.10 | Potash | 0.45 | 24 | 1.05 | 8.94 | 13297 | – |
| 4.11 | Potash | 0.45 | 39 | 2.20 | 9.03 | 13580 | – |
| 4.12 | Potash | 0.45 | 53 | 3.45 | 8.94 | 13284 | – |
| 7.2 | Steel | 0.5 | 18 | 0.50 | 6.5 | 6188 | 6254 |
| 7.3 | Steel | 0.5 | 38 | 1.55 | 6.68 | 6286 | – |
| 7.4 | Steel | 0.5 | 49 | 2.30 | 6.71 | 6369 | – |
| 7.9 | Glass | 0.5 | 18 | 0.55 | 7.03 | 7349 | – |
| 7.10 | Glass | 0.5 | 38 | 1.70 | 7.26 | 7466 | – |
| 7.11 | Glass | 0.5 | 49 | 2.50 | 7.29 | 7525 | – |
| 7.12 | Rimax | 1.0 | 30 | 0.65 | 3.95 | 2235 | 3342 |
| 7.13 | Rimax | 1.0 | 54 | 1.58 | 3.99 | 2290 | – |
| 7.14 | Rimax | 1.0 | 60 | 1.83 | 3.98 | 2224 | – |
| 7.15 | Rimax | 1.0 | 66 | 2.16 | 4.02 | 2320 | – |
| 7.16 | Rimax | 2.4 | 48 | 0.90 | 2.77 | 1086 | 1036 |
| 7.17 | Rimax | 2.4 | 60 | 1.25 | 2.80 | 1120 | – |
| 7.18 | Rimax | 2.4 | 84 | 2.2 | 2.87 | 1170 | – |

(1) The value of $b$ was reported by Smeulders *et al.* (1997). The conditions for the tests are given in table 1.

TABLE 2. Demonstration of the significant discrepancy between the available results. The conditions for the tests are given in table 1.

(1997) was about three times smaller than that obtained by our analysis (see table 1). Such a great difference is rather surprising especially when compared with the 5 % inaccuracy that was reported by the authors for their value of $b$, shown in square brackets in table 2. It should be noticed however, that such a high degree of inaccuracy could be the result of extrapolation and visual graphical estimation of the parameters measured in their tests: pressure drop, flow rate and inlet gas properties (Antohe *et al.* 1997). Our analysis is not subject to these effects. The sensitivity of the pressure history to the Forchheimer coefficient, $b$, is demonstrated in figure 6. It is evident that while the simulated results with the values of $b$ obtained using our analysis (dotted lines) agree excellently with the two recorded pressure traces, the simulated results

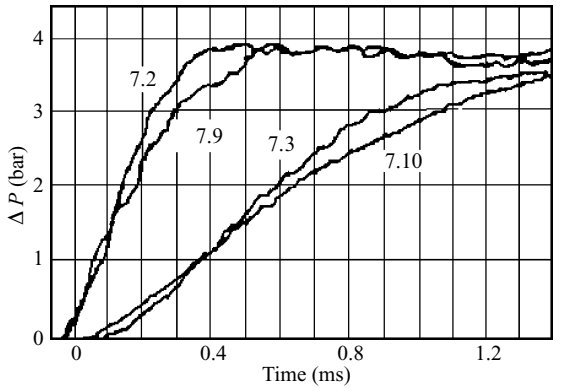


FIGURE 7. Endwall pressure traces measured with granular samples composed of glass and steel particles. The traces are numbered according to the test conditions listed in the table 2. For tests 7.2 and 7.9 $l = 18$ mm and for tests 7.3 and 7.10 $l = 38$ mm.

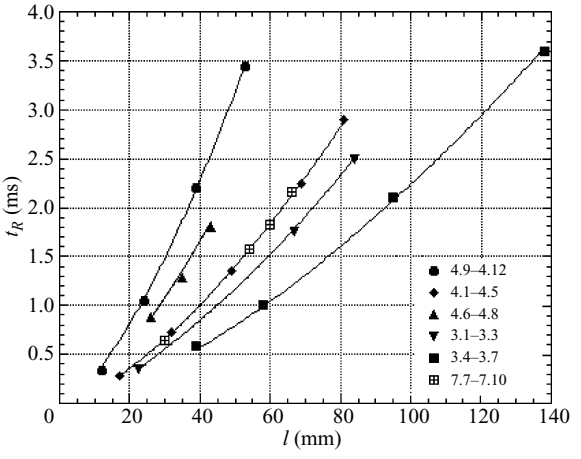


FIGURE 8. Measured values of the rise times, $t_R$, vs. sample length, $l$.

obtained by Ergun's coefficient (dashed lines) agree excellently with the results of test 1.1 while they completely miss the results of test 1.2.

Figure 7 shows examples of endwall pressure traces that are taken from Britan *et al.* (2001*a*). The expected sensitivity to the length of the granular sample is evident. However, as will be shown in figure 9, when presented in a non-dimensional form these pressure traces coincide since they correspond to the single value of $\chi = 1$. Note that in tests 7.2 and 7.9 the length was 18 mm while in tests 7.3 and 7.10 it was 38 mm. The small shift between curves of equal sample length is probably due to the change in the packing of the granular samples used in subsequent tests. The resulting values of $t_R$ after processing these pressure traces are listed in table 2. These results were then used for calculating the coefficients $K^F$ with the aid of equation (2.7). The rather small discrepancy (about 10 %) between the obtained values of $K^F$ that are shown in table 2 suggests that a Forchheimer-dominated flow had been established. If this is the case, equation (2.8) could be used to calculate the appropriate values of the Forchheimer coefficients, $b$, that are also shown in table 2.

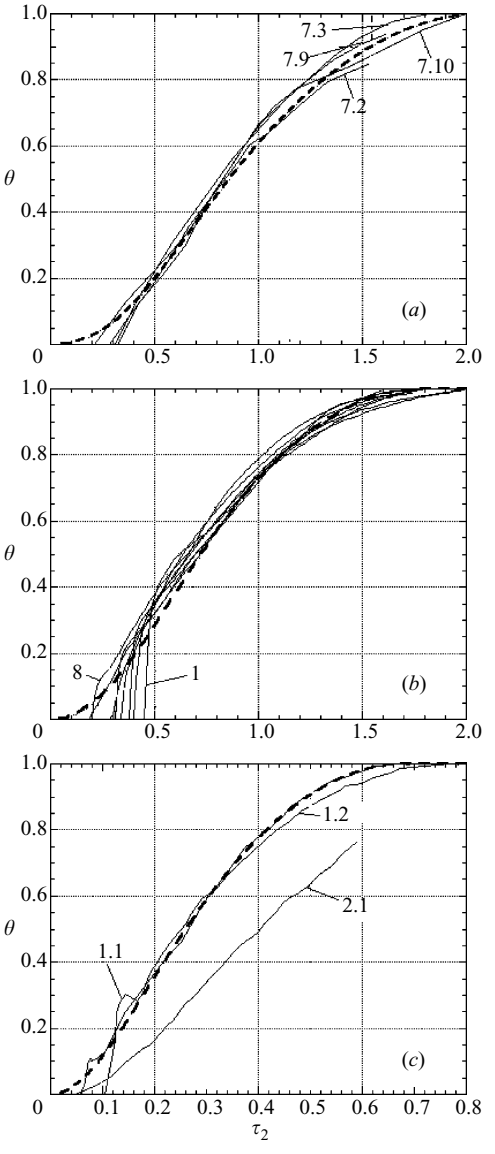


FIGURE 9. Generalized reproduction of the endwall pressure traces: (*a*) our results (the numbers labelling the curves refer to tables 1 and 2); (*b*) Levy *et al.*'s (1996, 1999) results (the numbers labelling the curves refer to table 3); (*c*) Smeulders *et al.*'s (1997) results (the numbers labelling the curves refer to tables 1 and 2).

To give another proof that the flows are indeed Forchheimer dominated the endwall pressure traces of experiments 3.1 to 3.7, 4.1 to 4.12 and 7.12 to 7.15 (see details in table 1) were analysed in a similar way. For the test conditions listed in table 1, the final results, which are shown by points in figure 8, were obtained as follows. Each of the $n$ recorded pressure traces was processed to obtain the rise times, $t_{R_i}$, as a function of the sample length, $l_i$. Thereafter, for each test in the series, which was conducted with a similar granular material, the coefficient $K_i^F$ was calculated using equation (2.7). The mean values of the coefficients, $\bar{K}^F = (1/n)\sum_1^n K_i^F$, were then used

| Test number | $M_s$ | $l$ [mm] | Material | $t_R$ [ms] | $K^F \times 10^3$ [ms/mm$^{1.5}$] | $b$ [m$^{-1}$] |
|---|---|---|---|---|---|---|
| 1 | 1.38 | 40 | SiC-10 | 0.40 | 1.58 | 390 |
| 2 | 1.38 | 60 | SIC-10 | 0.75 | 1.61 | 404 |
| 3 | 1.38 | 81 | SiC-10 | 1.20 | 1.65 | 425 |
| 4 | 1.38 | 41 | SiC-20 | 0.50 | 1.90 | 560 |
| 5 | 1.38 | 62 | SiC-20 | 0.90 | 1.84 | 530 |
| 6 | 1.38 | 83 | SiC-20 | 1.45 | 1.92 | 560 |
| 7 | 1.38 | 48 | $Al_2O_3$ | 0.68 | 2.04 | 648 |
| 8 | 1.38 | 93 | $Al_2O_3$ | 1.82 | 2.02 | 650 |

TABLE 3. Test conditions of the experiments of Levy *et al.* (1993, 1996).

as an input to calculated the curves $t_R = \bar{K}^F l^{1.5}$, which are shown in figure 8 by solid lines. Good agreement between the calculated curves and the points in this figure provide clear evidence that the shock-induced filtration, in these tests, satisfies the Forchheimer-flow conditions. By comparing the data of different series of experiments it can be easily seen that as predicted by equation (2.5), the rise time, $t_R$, indeed scales with the diameter of the particles, i.e. $t_R \sim (d_p)^{-0.5}$.

Figure 9($a$) presents a generalized reproduction of our results that were shown previously in figure 7. All four endwall pressure traces $P_w(t) - P_1$, when presented in the non-dimensional coordinates, $\theta\,|_{\chi=1}\,(\tau_2) = \theta_w(\tau_2)$, are grouped around the single limiting curve for Forchheimer-flow conditions. The manner in which the limiting curves (dashed lines) were calculated was explained while discussing figure 1.

The small deviation between the experiments for the initial part of the calculated curves is clear evidence of the diffusive character of equation (1.9$b$). When applying our analysis to the endwall pressure traces that were recorded by Levy, Ben Dor & Sorek (1993) and Levi *et al.* (1996) a similar behaviour is obtained (see figure 9$b$) in spite of the fact that their samples were not granular materials but solid SiC and $Al_2O_3$ porous materials (see table 3). The two pressure traces of Smeulders *et al.* (1997) that were shown in figure 6 are also grouped around the limiting curve in figure 9($c$). However, pressure trace 3 in figure 9($c$) (test 2.1 of table 1) that was also recorded by Smeulders *et al.* (1997) lies away from the common trend. According to the material characteristics that were reported by Smeulders *et al.* (1997), the conditions of this test (with smaller particles and a longer granular column) correspond to the mixed-flow domain (see figure 2). Therefore, the fact that this result does not group with the two others should not be surprising. Once the Forchheimer coefficient, $b$, of this test is evaluated a matching procedure between this pressure trace and the numerical solution of the common equation (1.8) would theoretically provide the means for estimating the Darcy coefficient, $a$.

Unfortunately, our estimates clearly show that the accuracy of the resulting coefficient, $a$, is low and could be increased only when the contribution of the viscous losses to the total energy losses increases. In this test as well as in the second test of the same series (van der Grinten *et al.* 1985), reproduced in figure 4, all the pressures were recorded close to the granular sample entrance where the contribution of the viscous losses was rather small.

The absence of suitable experiments motivated us to conduct a new test that complies with the developed mixed-flow conditions and has stronger viscous losses. This test is described and analysed in the next section.

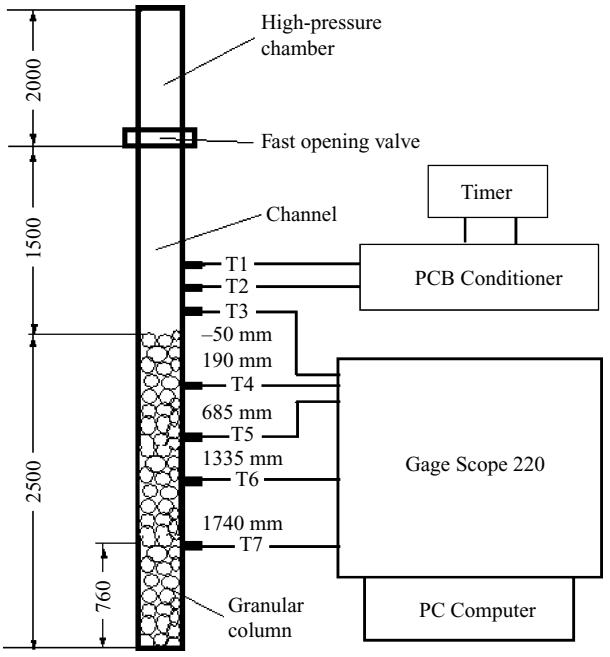


FIGURE 10. Schematic drawing of the shock tube and the data acquisition system. The locations of the pressure transducers T3 to T7 are measured from the front edge (entrance cross-section) of the granular column.

## 4. Evaluation of both the Darcy and the Forchheimer coefficients

### 4.1. *Experimental details*

The shock tube used for this test (figure 10) is a stainless steel cylindrical tube, having an internal diameter of 40 mm and a wall thickness of 8 mm. Its distinctive feature is a fast-acting valve, which replaces the traditional diaphragm technique as a mean of generating shock waves. In the valve design an auxiliary pressure chamber behind a light movable plastic piston is filled with the driving gas through a high-pressure inlet until the piston closes the passage from the high- to the low-pressure channel. The driver gas is then introduced into the high-pressure chamber until the required pressure is reached. The valve is activated by quickly dumping the gas inside the auxiliary pressure chamber. Owing to the suddenly imposed pressure difference between the atmospheric pressure in the low-pressure channel and the high driving pressure, the piston rapidly retreats. As a result, the high-pressure driver gas discharges immediately into the low-pressure channel, and a shock-wave is formed. The fast valve produces not only a sharp and well-defined shock wave, but also provides a very high repeatability of the shock-wave Mach number in air at ambient pressure (Britan *et al.* 2001*a*).

The shock tube channel has seven pressure ports and a buffer section, 76 cm long, which prevents unwanted edge effects from influencing the measurements. Two ICP (model 132A31) micro-sensors (T1 and T2 in figure 10) are flush mounted on the sidewall upstream of the granular column to measure the incident shock wave arrival times. These time measurements were used to calculate the shock-wave velocity just prior to its head-on collision with the front edge (entrance cross-section) of the granular sample. A PCB (model 113A) pressure transducer (T3 in figure 10) was used

as a reference pressure gauge to record the gas pressure at the entrance cross-section of the granular sample. The importance of the pressure recorded by this transducer, as it provides the actual boundary condition for the numerical simulation, will be outlined below. Four Kistler (model 603B1) pressure transducers (T4, T5, T6 and T7 in figure 10) were installed 190 mm, 685 mm, 1335 mm and 1740 mm downstream of the front edge to record the gas pressure histories at the side surface of the granular sample.

The pressure histories were transmitted through a PCB (model 442C04) conditioner and/or Kistler (model 5010B1) charge amplifiers and stored using a GageScope 250 data acquisition system, which had a sampling rate of 100 kHz per channel on a PC computer.

The rear edge (bottom) of the granular sample was placed against the rigid endwall of the test section, which enabled a quick assembly and an easy handling of loose packed natural sand ($d_p = 0.6$–$0.85$ mm).

### 4.2. *Gas dynamics analysis*

*The shock-tube flow*

The foregoing discussion implies that in experiments with long granular samples (when $t_R/\Delta t_5 > 1$), the dependence of the input pressure (i.e. the pressure acting on the entrance cross-section of the granular sample) must be accounted for, in order to correctly analyse the filtration flow process. To clarify this feature, we first simulated numerically the shock-tube flow upstream of the granular sample (for details see Britan, Vasiliev & Zinovick 1992). The initial conditions, at $t = 0$, were:

both the high- and the low-pressure chambers contained air ($\gamma_1 = 1.4$ and $\gamma_4 = 1.4$);

$$\left.\begin{array}{l} P_4 = 7.5\,\text{bar},\ T_4 = 300K,\ V_4 = 0 \text{ along } x \leqslant 2.0\,\text{m}, \\ P_1 = 1.0\,\text{bar},\ T_1 = 300K,\ V_1 = 0 \text{ along } 2.0 < x \leqslant 3.5\,\text{m}, \end{array}\right\} \tag{4.1}$$

where the subscripts 1 and 4 correspond to the initial gas conditions in the low- and the high-pressure chambers, respectively.

Figure 11 shows the $(x, t)$-diagram of the flow process as calculated numerically using the 'classical' shock-tube theory for an ideal inviscid flow, for the case of $M_s = 1.49$. Figure 12 shows the numerically simulated $(a, c)$ and experimentally recorded $(b, d)$ sidewall pressure histories at the pressure port T3 (see figure 10) located 50 mm upstream of the front edge (entrance) of the granular sample. The main differences between the measured and simulated flow fields in the four parts of this figure probably arise from the fact that in the 'classical' shock-tube theory the flow is initiated by instantaneously rupturing an infinitely thin diaphragm that separates the high- and low-pressure chambers, and the incident shock wave reflects at a solid endwall, while in our shock tube, a fast opening valve replaces the diaphragm and the incident shock wave reflects from the porous front edge of a granular sample.

The flow states ahead of the incident shock wave, behind the incident shock wave, behind the incident rarefaction wave, ahead of the incident rarefaction wave and behind the shock wave that was reflected at the front edge of the granular sample are labelled (1), (2), (3), (4) and (5), respectively in figure 11. Corresponding letters mark the times of arrival of the various waves at the front edge of the granular sample, which is located at $x = 3.5$ m. Points A represent the time of arrival of the incident shock wave at the front edge of the granular sample. At this moment the pressure jumps from $P_1$ to $P_5$ (figure 12). Point B, which marks the arrival of the shock wave that is reflected from the contact surface, restricts the test time period, as suggested by the classical shock tube theory, to $\Delta t_5 = 2$ ms. The arrival of the rarefaction wave,

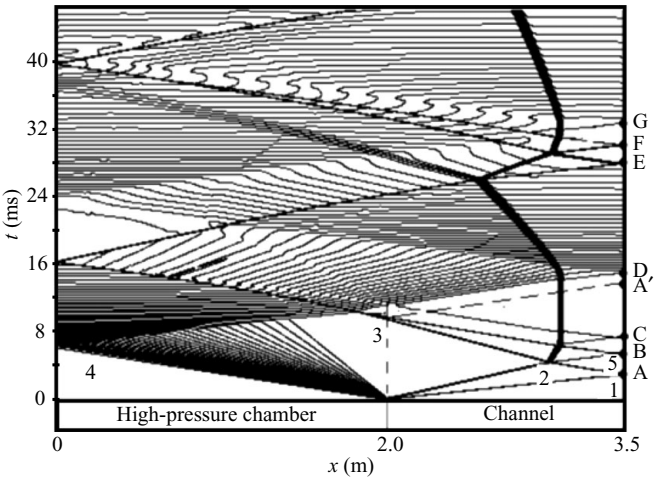


FIGURE 11. A numerically generated $(x, t)$ diagram illustrating the waves bouncing back and forth inside a 'classical' shock tube and the granular sample, and their interaction with each other. The high- and low-pressure chambers were filled with air at 7.5 bar and 1.0 bar, respectively. The initial temperatures in both chambers were 300 K. The incident shock wave Mach number was 1.49.

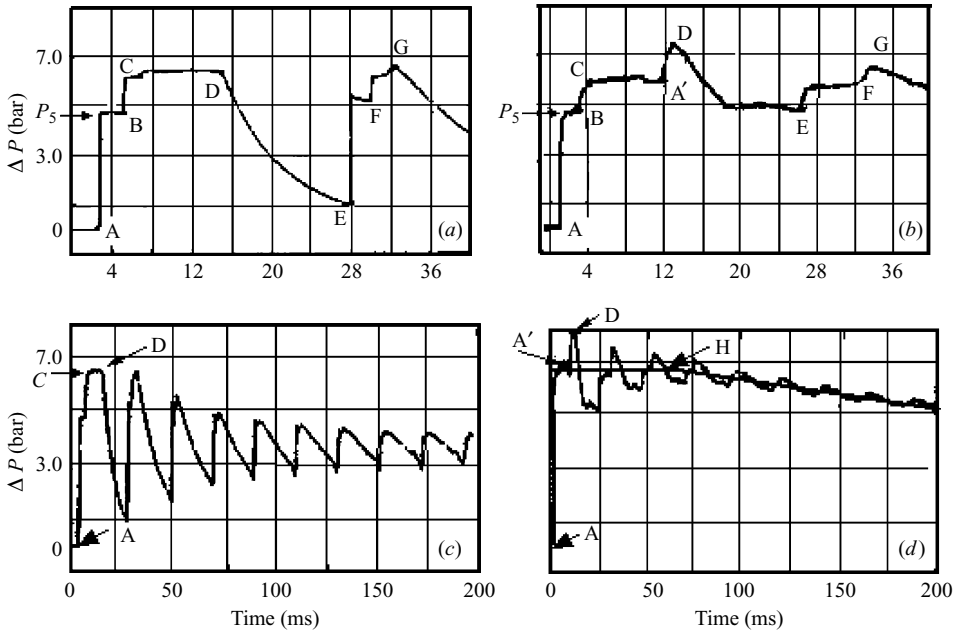


FIGURE 12. The numerically simulated $(a, c)$ and recorded $(b, d)$ sidewall pressure histories at the pressure port T3, that is located 50 mm upstream of the front edge (entrance) of the granular sample (see figure 10).

marked as point D, significantly reduces the pressure at the entrance cross-section of the granular sample both in the simulation and in the experiment. At this stage, the rarefaction wave that was reflected earlier from the endwall of the high-pressure chamber has reached the test section. The pressure jumps marked by points E, F

and G are the result of *refraction* of the main reflected shock wave at the contact surface. An inspection of figures 12(*a*) and 12(*b*) indicates that the simulated and the measured pressure histories correlate well until the arrival of the shock wave (not resolved by the simulations) reflected from the fast valve and recorded in figure 12(*b*) as point A′.

The above analysis reveals the following important features of the pressure field in the vicinity of the front edge of the granular sample.

1. The recorded pressure acting on the front edge of the granular sample is different from that predicted by the classical shock-tube theory.

2. The length of the shock tube determines the duration of the pressure oscillations, which are well predicted by the theory and are caused by subsequent back and forth propagation of the shock and the rarefaction waves.

3. The peak-to-peak amplitude of the simulated pressure pulsations is symmetrical and attenuates rather slowly. In contrast, the amplitude of the recorded pulsations quickly decays, while the mean pressure level initially remains constant during the first 60 ms and then starts to drop linearly in time (after point H in figure 12*d*).

4. The fast opening valve also contributes to the difference between the measured and the simulated pressure histories. This is because the reflected shock wave interacts with the valve and gives rise to a new shock wave that is directed towards the front edge of the granular sample. This wave, which does not exist in simulations based on the 'classical' shock-tube theory, provides additional compression of the gas flow and supports the higher level of the recorded pressure inside the granular sample.

*Filtration flow through a granular sample*

The unsteady input pressure presented above, which acts on the entrance cross-section of the granular sample, controls the filtration flow within the granular sample. To better understand the nature of the filtration flow, the propagation of the main disturbances along the granular sample must be considered. This could be done by solving numerically equation (1.6) or (1.8). However, instead of applying the actual boundary conditions (see figure 12*d*) the following approximated boundary conditions, shown by a thin solid curve in figure 12(*d*), were used:

for the quasi-steady period between points A and H ($0 \leqslant t \leqslant 60$ ms)

$$\Delta P(t) = 6.5 \text{ bar}; \tag{4.2}$$

for the linear pressure drop after point H ($t \geqslant 60$ ms)

$$\Delta P(t) = 6.5 - 0.0083(t - 60) \text{ bar}. \tag{4.3}$$

The resulting $(x, t)$-diagram for this case is shown in figure 13. It is evident that the filtration starts following the passage of the transmitted wave (TW) that separates the undisturbed gas in the pores (1) and gas that has already been compressed by the transmitted wave (2*). To eliminate confusion with the notation of the domains in figure 11, the regions behind the transmitted and reflected waves are denoted, respectively, by (2*) and (5*) in figure 13. The trajectory of the contact surface, CS, separates the filtration flows into two different domains. Domain (2*) contains relatively cold gas that initially occupied the pores of the sample and then was compressed by the transmitted wave (TW). Subsequently, the gas that occupied domains (6) and (7) was originally compressed and heated by the reflected shock wave outside of the granular sample (see region 5 in the $(x, t)$-diagram in figure 11).

An inspection of figure 13 indicates that the resulting history of the interstitial flow has several stages. During the quasi-steady period restricted by point H and prior to

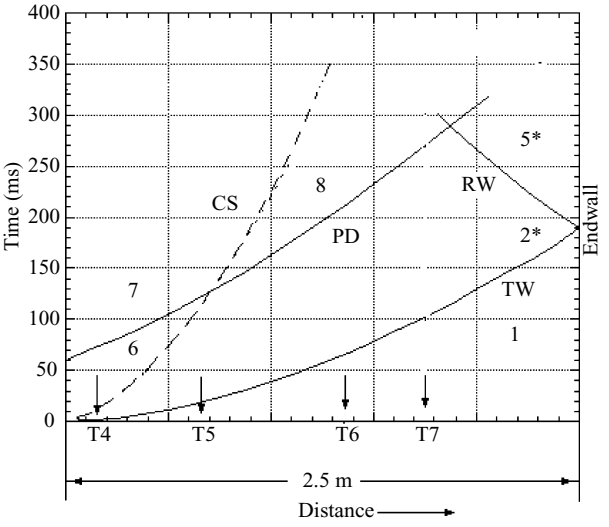


FIGURE 13. A numerically generated $(x, t)$-diagram illustrating the wave propagation through a granular sample composed of 0.5 mm sand particles. TW-transmitted wave, RW-reflected wave, CS-contact surface, PD – pressure decay front.

the arrival of the transmitted wave at the endwall, the flow behaves as if the sample has an infinite length. The transmitted wave quickly decays (see figure 13), and thus, it induces behind it an unsteady pressure that is indicative of the reducing capacity of the granular sample. However, once the transmitted shock wave is reflected from the endwall, the gas filtration cannot be treated independently of the rear end of the sample. The transient pressure drop at the front edge of the granular sample further complicates the problem. Starting from point H at the granular sample interface, the information on the transient pressure drop moves over the granular sample (see the trajectory marked by PD) and modifies the filtration flow at this stage. When applied to the main problem considered here it is therefore of interest to know to what extent these modifications in the flow conditions affect the values of the Darcy and the Forchheimer coefficients ($a$ and $b$) that were obtained using the hybrid method. This question has been tested in two different aspects, as described in the following section.

One aspect is the sensitivity of the interstitial flow pressure to the sharp fluctuations of the input pressure. To better illustrate this aspect, we first present in figure 14($a$) all the pressure traces that were recorded in our tests upstream and inside the granular sample. The figure also includes black circular points that mark the times of arrival of the pressure drop at the subsequent pressure port.

(i) Pressure trace T4 clearly demonstrates that the arrival of the reduced input pressure indeed affects the filtration. In fact, at the point marked with a black circle the initial pressure rise is levelled out and then shows little or no change over this value, which is much smaller than the recovering level. Notice that outside the granular sample (see trace T3), the input pressure decayed faster and the amplitude of the pressure trace T4 ultimately exceeded the final level of the pressure trace T3.

(ii) Owing to the damping capacity of the granular material, sharp variations of the input pressure inside the bulk became smooth and weak. The stepwise front and further fluctuations of the input pressure signal T3 were changed inside the granular sample to a gradual pressure rise in traces T5, T6 and T7. Note also the small fluctuations of the amplitude in the pressure trace T4. These fluctuations represent

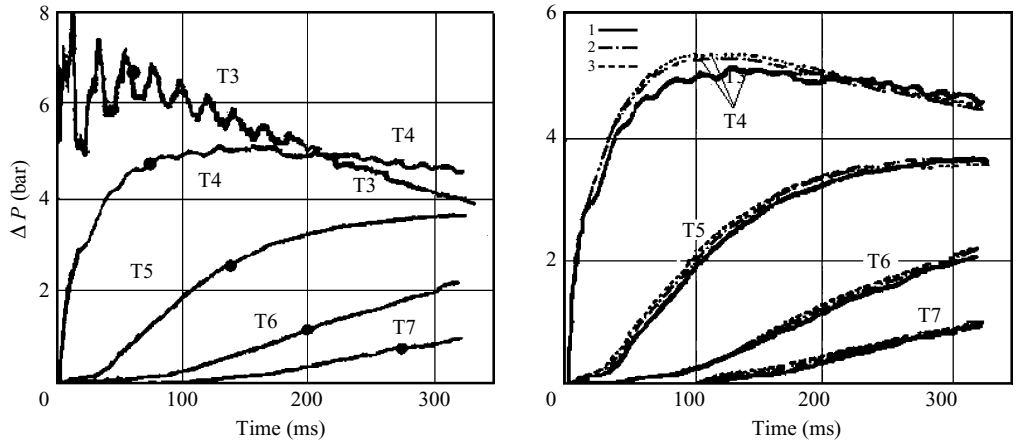


FIGURE 14. (*a*) Pressure traces recorded in our tests upstream of and inside a granular sample of sand. The black circular points mark the times of arrival of the pressure drop, PD, to the pressure port. (*b*) Comparison between (1) the registered pressure traces; (2) their simulations based on the simplified model; and (3) the full solution of Britan *et al.* (2006).

only weak responses to the strong tooth-shaped oscillations of the input pressure T3. Similarly, while the time of arrival of the reduced input pressure is discernible as a weak inflection point in the pressure traces T4 and T5, this has no impact on the dynamics of the downstream pressure traces T6 and T7.

(iii) Combining the results shown in figures 12(*d*) and 13 reveals that the quasi-steady input conditions between points A and H control the filtration flow in domains (2*) and (6). In considering these domains, the pressure field could be described by equations (1.6) or (1.8). Once the signals of the input pressure drop reach the relevant pressure port (see the inflection point (H) in figure 12*d*), the filtration flow in domains (7) and (8) starts to depend on the unsteady input conditions. From this time on, equations (1.6) or (1.8) have to be solved under unsteady input conditions.

Another aspect to be characterized is the so-called 'temperature effect' or sensitivity of the pressure field to the different temperature of the gas flow. Previous analysis of the trajectory (CS) in figure 13 reveals that the gas flow acting on the pressure transducers at ports T6 and T7 for a long time period is composed of the relatively cold gas of domain (2*). Consequently, the filtration process at ports T6 and T7 better corresponds to the isothermal model of filtration, which was suggested by Morrison (1972, 1976, 1977). By contrast, the temperature of the gas in domains (6) and (7) and acting on the pressure transducers at ports T4 and T5 is much higher. Therefore, the resulting heat transfer at ports T4 and T5 could cause deviations of the pressure field from the one predicted by the simplified model. These deviations (if they exist) could be evaluated using computer modelling based on our so-called full-solution code (Britan *et al.* 2006). To confirm this, two numerical simulations of the recorded pressure traces, one using the simplified model (equation (1.8)) and another one using the just-mentioned full-solution code, were conducted. Figure 14(*b*) summarizes the results of this analysis, where the registered pressure traces (curves 1) are compared with simulations based on the simplified model (curves 2) and on full-solution code (curves 3). Note that to resolve the unsteady system of conservation equations including the heat transfer effect the full-solution code requires several hours/run while the simplified solution needs less than 0.2 hours/run. In spite of this

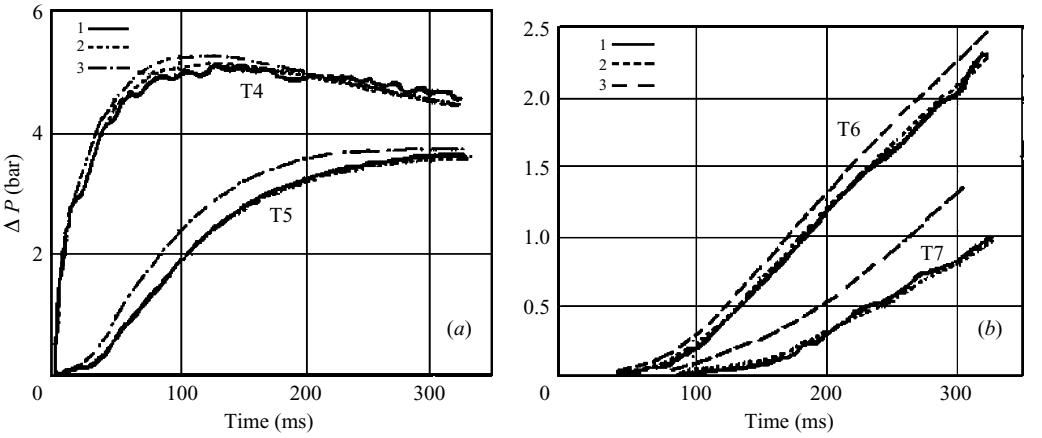


FIGURE 15. (*a*) Comparison between the recorded pressure traces T4 and T5 (1) and two numerical simulations: (2) solutions of equation (1.9*b*) with $b = 8250\,\mathrm{m}^{-1}$; (3) solution of equations (1.8) and (1.9*b*) using Ergun's coefficients, $a = a_0$ and $b = b_0 = 6000\,\mathrm{m}^{-1}$. (*b*) Comparison between the recorded pressure traces T6 and T7 (1) and two numerical simulations: (2) solution of the common equation (1.8) with $a = 2.7 \times 10^9\,\mathrm{m}^{-2}$ and $b = 8250\,\mathrm{m}^{-1}$; (3) solution of equation (1.9*b*) with $b = 8250\,\mathrm{m}^{-1}$.

fact the two corresponding curves almost completely coincide and the agreement with the registered pressure traces is quite good. It is therefore concluded that the effect of high temperature on the pressure profiles is negligibly small.

### 4.3. *Matching procedure and scaling of the pressure profiles*

The foregoing discussion, which was aimed at determining both the Darcy and the Forchheimer coefficients, is sufficient to enable one to definitely conclude that the pressure ports T4 and T5 could be used as a base to specify the Forchheimer coefficient, *b*. The main results that demonstrate the steps of the matching procedure, which specifies this coefficient, are shown in figures 15(*a*) and 15(*b*). Two questions must be answered at this stage:

Do the pressure profiles at least at the locations of the T4 and T5 transducers correspond to the Forchheimer regime?

Does Ergun's (1952) correlation give, in our case, acceptable agreement with the measursed pressure histories?

For this purpose the numerical solutions of equations (1.8) and (1.9*b*) using Ergun's coefficients, $a = a_0 = 2.0 \times 10^9\,\mathrm{m}^{-2} =$ and $b = b_0 = 6000\,\mathrm{m}^{-1}$ (see relations (1.2*a*) and (1.2*b*) and approximations (4.2) and (4.3) for the boundary conditions were generated. For each of the pressure ports T4 and T5 the resulted pair of curves that corresponds to equations (1.8) or (1.9*b*) are so closely spaced that they could be considered as a single curve (see curves 3 in figure 15*a*). Recall that the solution of equation (1.9*b*) describes the pressure history in a Forchheimer-dominated flow while the common equation (1.8) complies with a mixed-flow regime. Hence, close correlation between those two solutions reveals the negligibly small role of viscosity and thus provides support that Forchheimer flow conditions exist at pressure ports T4 and T5.

The answer to the second question can be found by comparing the numerically simulated pressure curves to the experiment. The experimental pressure traces in figure 15(*a*) demonstrate that the numerical solution (curve 3) failed to predict accurately enough the pressure trace registered at port T5. Such a discrepancy strongly suggests that the value of the Forchheimer coefficient $b = 6000\,\mathrm{m}^{-1}$ used in

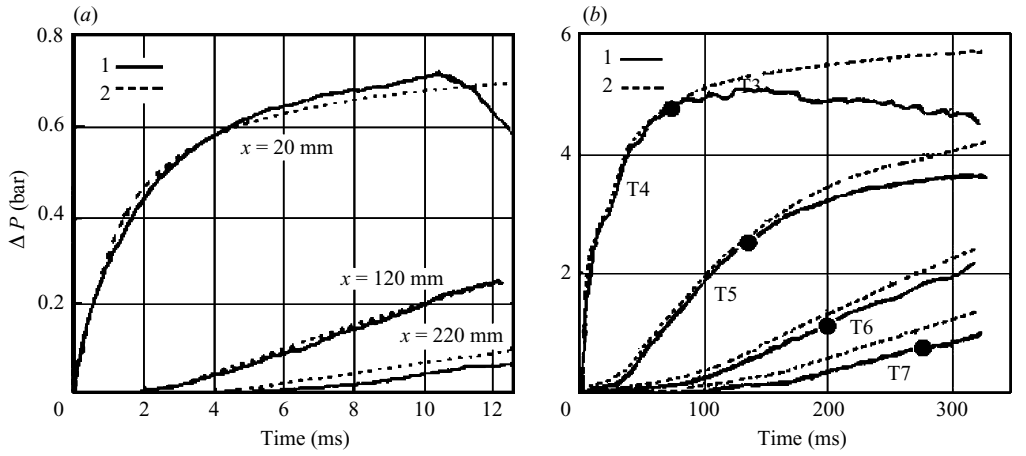


FIGURE 16. (*a*) Comparison between the measured (1) and reconstructed (2) pressure traces for the experiments of van der Grinten *et al.* (1985), and (*b*) the controlled test of the present study. The black circles mark the times of arrival of the pressure drop at the pressure port.

the calculations of curves (3) should be corrected. To find the new, corrected value of $b$ a standard matching procedure was employed when the pressure trace recorded at port T5 was compared to the results of a series of solutions of equation (1.9*b*) with different values of $b$. As a final stage of this procedure, curves (2) which were obtained by using $b = 8250\,\mathrm{m}^{-1}$ provided the optimal matching to the two measured pressure traces, T5 and T4. Consequently, the value $b = 8250\,\mathrm{m}^{-1}$ was adopted as the correct Forchheimer coefficient.

Further inspection of the figure 15(*b*) shows, however, that the numerical solution of equation (1.9*b*) with the just-established corrected value of the Forchheimer coefficient $b = 8250\,\mathrm{m}^{-1}$ failed to predict the downstream pressure records T6 and T7. The evident discrepancy between the experiments (solid lines 1) and the simulations (dashed lines 3) implies that at least, at port T7, the filtration most likely complied with the mixed-flow domain rather than the Forchheimer-flow domain. To confirm this, the pressure trace recorded at port T7 was simulated using the common equation (1.8) with $b = 8250\,\mathrm{m}^{-1}$ and a series of different values of the coefficient $a$. The sample of the results in figure 15(*b*) suggested that the optimal matching to the recorded pressure T7 (curve 1) was provided by the numerically predicted pressure trace (2) calculated with $a = 2.7 \times 10^9\,\mathrm{m}^{-2}$ and $b = 8250\,\mathrm{m}^{-1}$. These coefficients also improved the agreement between the predicted (curve 2) and the recorded (1) pressure traces at port T6.

In order to support the scaling procedure that was presented in § 2.2, as the first example, the experimentally recorded pressure traces previously shown in figure 4 were selected because the input load in this test was close to being constant during the entire test time (about 10 ms). Hence, the tested conditions complied well with the steady-state approximation of the method. The recorded pressure traces of figure 4 are reproduced again in figure 16(*a*) and compared with the results of the scaling procedure. As the basis for the scaling, the numerical solution of equation (1.9*b*) was generated first to obtain the additional pressure history at the cross-section located at $x = 10$ mm (not shown in this figure). Since the filtration flow was assumed to comply with the Forchheimer domain, the exponent in relation (1.11) used for the scaling was assigned the value $j = 1.5$. As expected, the agreement between the experimental (1) and the reconstructed (2) pressure histories was very good at

the distances $x = 20$ mm and $x = 120$ mm. This suggested that the filtration flow at both pressure ports was indeed of Forchheimer type. In addition, the fact that the scaling procedure overestimated the pressure history at $x = 220$ mm, suggested that this pressure port was positioned downstream of the domain appropriate to the Forchheimer-flow conditions and hence, most likely, corresponded to the mixed-flow domain.

As the next example for the scaling procedure, the results of our controlled laboratory test previously shown in figure 14(*b*) were chosen. In figure 16(*b*) the pressure traces recorded at the pressure ports T4 to T7 are reproduced again as solid lines (1). As a basis for the scaling for this case the calculated pressure history at $x = 50$ mm (not shown) was used. Recall that the scaling procedure was capable of reproducing the experiment as long as the input conditions were steady. Although the quasi-steady approximation (when, as can be seen in figure 12(*d*), the input pressure was nearly constant) was considered to hold during the first 60 ms of our test, the pressure drop that occurred at the input afterwards was eventually picked up at the pressure ports downstream of the entrance. Hence, an interesting issue to evaluate was the related deviation of the reconstructed pressure profiles (curves 2) from the measured pressure traces (curves 1). In figure 16(*b*) this effect can be understood by inspecting the black circular points that represent the trajectory of the pressure drop (PD) of figure 13. As expected, the error in the scaling procedure appeared when the pressure drop that was transmitted into the granular sample reached the related pressure port. However, even prior to this moment, the scaling in figure 16(*b*) worked quite well only at the first two pressure ports, T4 and T5, and it overestimated the pressures recorded further downstream. This is consistent with our previous conclusion that the flow at the pressure ports T4 and T5 complied with the Forchheimer-flow domain, while the flow at ports T6 and T7 was closer to being in the mixed-flow domain.

### 4.4. *Evaluation of the Darcy coefficient using small-scale tests*

The above example clearly showed that a direct matching of the theory to a shock-tube test could give the coefficient $a$ if the coefficient $b$ was specified or known in advance and the filtration flow complied with the mixed-flow conditions. Since apart from our last experiments, we failed to find in the literature other shock-tube tests that comply with the mixed-flow conditions, let us refer to the combustion test of Asay *et al.* (1996). In their experimental set-up, shown in figure 17(*a*), the burning products of the HMX explosive penetrated into a short packed bed of inert SiC powder having porosity of $\varepsilon \approx 0.26$. The pressure sweep in figure 17(*b*) started at $t = 0$ when a voltage (12 V) was applied to the Profuse. After several milliseconds, the HMX grains ignited and the pressure T1 in the burn chamber began to rise. The recorded pressure histories at ports T2 to T4 showed the filtration phenomenon of the burning products through the packed bed. This figure reveals that the extremely high and sharp input pressure in the burn chamber (about 3200 bar) quickly turned into weak and smooth pressure traces as it moved downstream along the packed bed (see the pressure traces T2, T3 and T4). This result is consistent with another important finding that was extracted by Asay *et al.* (1996) from their numerical simulations of the filtration phenomenon: when a rapid flow of the hot burning products entered the front edge of the packed bed, the input temperature (about 4000 K) dropped so quickly that after propagating a distance of about 3 mm downstream it reached about 400 K. This meant that gas filtration in Asay *et al.*'s (1996) experiment could be considered as occurring under a constant temperature close to the room temperature. Notice that the diameter of the granules, $d_p$, that were used in their test, 1–5 μm, was more than

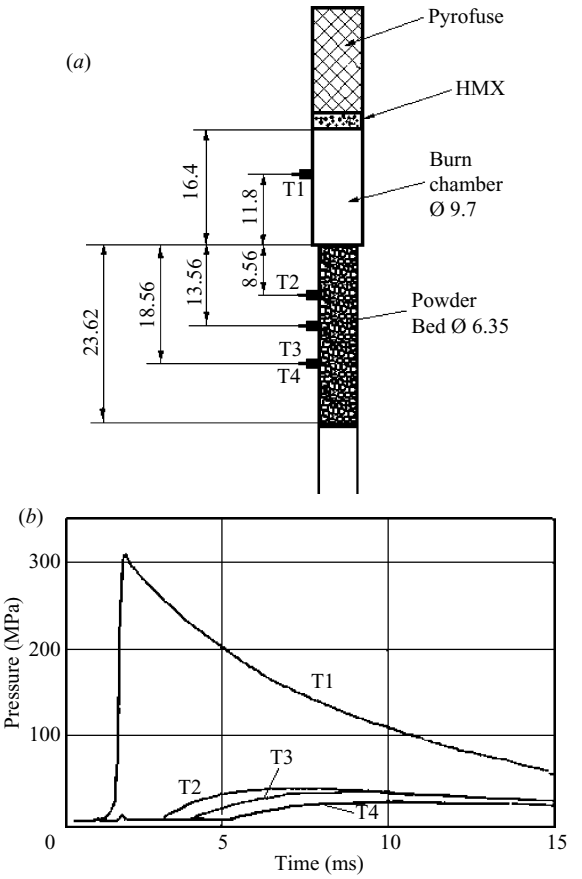


FIGURE 17. (*a*) Schematic of the combustion test of Asay *et al.* 1995). (*b*) Typical pressure traces measured during the combustion test at the entrance (T1) and inside (T2 to T4) the packed bed of Asay *et al.* (1995).

three orders of magnitude smaller than the smallest particle listed in table 1. Since based on equation (2.1) the Reynolds number was extremely small, about $Re_f \approx 10^{-6}$, isothermal Darcy flow conditions existed over most of the packed bed. Moreover, in an attempt to avoid the complexities involved at the packed bed interface, Asay *et al.* (1996) used as a left-hand boundary condition the measured pressure trace T2 and then specified the required macroscopic parameter of the filtration flow using the pressure trace T3. Leaving aside the details of their data processing, it should be noted that the matching procedure used by Asay *et al.* (1996) is sensitive to the input parameters of their test. In fact, extremely high impact pressure inevitably results in local changes in the packed bed porosity, $\varepsilon$, in addition to the possible changes in the viscosity of the gas flow, $\mu$, due to the high temperatures. Since the proposed hybrid method does not include these mechanisms, analysis of filtration driven by extremely high impact conditions through micron-sized materials needs a more complicated theory and special tests.

In contrast, in most problems related to blast wave/structure interaction, the impact is far from extremely high and the granular material is usually composed of sand-sized particles. Experiments that eliminate the need for long samples while complying with the mixed- or Darcy-flow conditions over a significant part of the granular

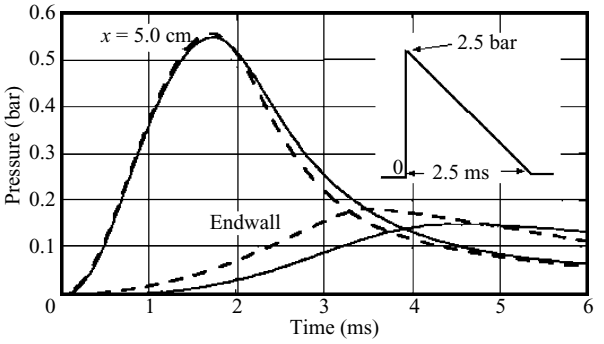


FIGURE 18. Typical results demonstrating the numerical design of the controlled shock tube tests. Dashed lines – numerical solution of equation (1.9*b*) for a Forchheimer-dominated flow. Solid lines – numerical solution of the common equation (1.8) for a mixed flow.

bed could be of interest. Formal analogy with the experiment of Asay *et al.* (1996) suggests for this purpose a shock-tube test with a continuous pressure drop at the input to the granular bed. This pressure drop has to complement the viscous losses to reduce of the interstitial velocity, $\tilde{V}$, and could be easily achieved by allowing the rarefaction wave to overtake the incident shock wave. It is clear that if the overtaking takes place before the time moment marked as (A) in figure 11, the rarefaction wave will dominate the pressure fields behind the incident and the reflected shock waves. To realize this scenario in a controlled shock-tube test with a triangular, blast-shaped pressure profile at the front edge of the granular sample, the length of the high-pressure chamber should be reduced to several centimetres (Britan *et al.* 1991). To verify this we focused on the simulated parameters of gas filtration through a standard 200 mm long granular sample that is composed of loose packed spheres having a diameter $d_p = 0.5$ mm and porosity $\varepsilon = 0.4$. Correlations (1.2*a*) and (1.2*b*) for this case resulted in the following values of Ergun's coefficients: $a_0 = 16.2 \times 10^8\ \mathrm{m}^{-2}$ and $b_0 = 5400\ \mathrm{m}^{-1}$. As boundary conditions, we used the following approximation of the pressure trace that was measured and reported by Britan *et al.* (1991):

$$\text{for } 0 \leqslant t \leqslant \Delta t \quad \Delta P_5(t) = 2.35\left(\frac{t}{\Delta t}\right) \text{ bar}, \quad \Delta t = 2.5\,\text{ms},$$
$$\text{for } t < 0 \quad \text{and} \quad t > \Delta t \qquad \Delta P = 0.$$

As a result, the pressure profiles obtained from a series of solutions of the common equation (1.8) and equation (1.9*b*) are compared to each other in figure 18 where the inset represents the input pressure profile. Like the data in figure 15 the coincidence of the two solutions (in this figure it is at a distance of $x = 5$ cm inside the granular sample), indicates that Forchheimer-flow conditions were established. Hence, using a trial-and-error method for matching these pressure traces and the experiment, one could specify the coefficient $b$. If significant differences exist between the two solutions at the endwall it means that mixed-flow conditions were established there. Then, the known value of the coefficient $b$ and the matching procedure applied to the endwall pressure traces specify the required coefficient $a$.

## 5. Summary and discussion

In the context of the so-called hybrid method the work presented here has demonstrated the contribution of shock tubes to the problem of shock-induced filtration of the gas flow through granular media. An important feature of the hybrid method is that the common behaviours of the filtration process become visible naturally using a simplified approach to the problem. In this way, the use of the simple calculation, in itself, provides insight into the mechanisms of the filtration in addition to that provided by controlled laboratory tests. In order for the hybrid method to become a quantitative tool for practical applications, a calibration of the simplified model of gas filtration with respect to available and new controlled shock-tube data was performed. The main results of this method are as follows:

1. Conventional shock tubes yield quantitative information on the pressure field inside granular samples that could be used only for simulating flows that satisfy the Forchheimer-flow conditions (i.e. relatively short granular samples).

2. The boundaries between the three possible flow domains (Forchheimer, mixed and Darcy flow) were identified. This complements the work of Morrison (1972, 1976, 1977) in which these boundaries were not specified.

3. In order to determine the key coefficient, namely the Forchheimer coefficient, $b$, we have implemented a special procedure that combined a series of numerical experiments and controlled laboratory tests.

4. A scaling procedure that enables one to reconstruct the pressure histories at different locations along the granular sample, during the steady period of the input conditions, by using a single measured pressure trace was suggested.

5. A simplified treatment of the wave process upstream and within a long (2.5 m) sample of natural sand was conducted. Approximations (4.2) and (4.3) that were applied, in the course of the present analysis, to the pressure trace recorded at the front edge (entrance) of the sample allowed the test-time period to be extended to several hundreds of microseconds. The two key parameters, the Darcy and the Forchheimer coefficients, could be determined by applying a matching procedure between the experimentally recorded and numerically simulated pressure traces within the sample.

6. As an alternative to these unusual measures (a long granular sample and extended test time period) a new design of a controlled shock tube test with the Forchheimer- and mixed-flow regimes that could be obtained with a standard granular sample was suggested.

This study was conducted under the auspices of the Dr Morton and Toby Mower Professorial Chair of Shock Wave Studies. The authors acknowledge the Israel Science Foundation (Grants No.278/03, No.154/04) for financial support which made this research possible.

## REFERENCES

Antohe, B. V., Lage, J. L., Price, D. C. & Weber, R. M. 1997 Experimental determination of permeability and inertia coefficients of mechanically compressed aluminum porous matrices. *Trans. ASME*: *J. Fluids Engng* **119**, 404–412.

Asay, B. W., Son, S. F. & Bdzil, J. B. 1996 The role of gas permeation in convective burning. *Intl J. Multiphase Flow* **22**, 923–952.

Britan, A., Ben-Dor, G., Elperin, T., Igra, O. & Jiang, J. P. 1997 Gas filtration during the impact of weak shock waves on granular columns. *Intl J. Multiphase Flow* **23**, 473–491.

Britan, A., Ben-Dor, G., Igra, O. & Shapiro, H. 2001*a* Shock waves attenuation by granular filters. *Intl J. Multiphase Flow* **27**, 617–634.

Britan, A., Ben-Dor, G., Igra O. & Shapiro, H. 2006 Development of a general approach for predicting the pressure fields of unsteady gas flows through granular media. *J. Appl. Phys.* **99**(9), 093519.

Britan, A., Ben-Dor, G. & Shapiro, H. 2001*b* Numerical and analytical investigations of the head-on interaction of shock waves with granular layers. *In Proc. 23rd Intl Symp. Shock Waves, Univ. Texas, Arlington, USA*, p. 210.

Britan, A. & Levy, A. 2001 Weak shock wave interaction with inert granular media. In *Handbook of Shock Waves* (ed. G. Ben-Dor, O. Igra & T. Elperin), vol. 2, pp. 597–666. Academic.

Britan, A., Vasiliev, E. I. & Zinovik, I. 1992*a* Reflection of a blast profile shock wave from the end-wall of a shock tube. *Fluid Dyn. USSR* **3**, 412–417.

Britan, A., Vasiliev, E. I. Zinovik, I. & Kaminin, I. 1992*b* Reflection of blast-profile shock wave from the end wall of a shock tube. *Fluid Dyn.* **3**, 412–417.

Engebretsen, T., Bakken, J., Hansen, E. W. M. & Lysberg, I. 1996 Shock waves and gas flow through granular materials. In *Proc. Workshop Explosion Effects in Granular Materials* (ed. A. Jenssen, H. Langberg & C. Madshus), Oslo, Norway, pp. 111–131.

Ergun, S. 1952 Fluid flow through packed columns. *Chem. Engng Prog* **48**, 89–73.

Gelfand, B. E., Medvedev, S. P., Borisov, A. A., Polenov, A. N., Frolov, S. M. & Tsyganov, S. A. 1989 Shock loading of stratified dusty system. *Combustion* **9**, 153–165.

van der Grinten, J. G. M., van Dongen, M. E. H. & van der Kogel, H. 1985 A shock-tube technique for studying pore-pressure propagation in dry and water-saturated porous medium. *J. Appl. Phys.* **58**, 2937–2942.

Holman, J. P. 1994 *Experimental Methods for Engineers*, 6th Edn. McGraw-Hill.

Lage, J. L. 1998 The fundamental theory of flow through permeable media. From Darcy to turbulence. In *Transport Phenomena in Porous Media* (ed. D. B. Ingham & I. Pop), pp. 1–30. Pergamon.

Lage, J. L. & Antohe, B. V. 2000 Darcy's experiments and the deviation to nonlinear flow regime. *Trans. ASME. J. Fluids Engng* **122**, 619–625.

Levy, A. 1999 Shock wave interaction with granular materials. *Powder Tech.* **103**, 212–219.

Levy, A., Ben Dor, G. & Sorek, S. 1993 Head on collision of normal shock waves with rigid porous materials. *Exps. Fluids* **15**, 183–190.

Levy, A., Ben Dor, G. & Sorek, S. 1996 Numerical investigation of the propagation of shock waves in rigid porous materials: development of the computer code and comparison with experimental results. *J. Fluid Mech.* **324**, 163–179.

Levi, A., Levi-Hevroni, D., Sorek, S. & Ben-Dor, G. 1999 Derivation of Forchheimer terms and their verification by application to waves propagation in porous media. *Intl J. Multiphase Flow* **25**, 683–704.

Liang, S-F. & Chao, Z. 1998 *Principles of Gas-Solid Flows*. Cambridge University Press.

Macdonald, M. S., El-Sayed, M. S., Mourg K. & Dullien, F. A. L. 1979 Flow-through porous media – the Ergun equation revisited. *Ind. Engng Chem. Fundam.* **18**, 199–208.

Medvedev, S. P., Frolov, S. M. & Gelfand, B. E. 1990 Shock wave attenuation by screens composed of granular materials. *Engng Phys. J. (USSR)*, **55** (6), 924–928 (in Russian).

Mikami, H., Kanada, T., Sakumara, Y. & Susuki, T. 2001 Pressure waves in a shock loaded dust layer. In *Proc. 23rd Intl Symp. Shock Waves, Univ. Texas, Arlington, USA*, pp. 834–840.

Morrison, F. A. 1972 Transient gas flow in a porous column. *Ind. Engng Chem. Fundam.* **11**(2), 191–197.

Morrison, F. A. 1976 Similarity in transient high-speed gas flow through porous media. *Trans. ASME*: *J. Fluids Engng* **8**, 567–568.

Morrison, F. A. 1977 Transient non-Darcy gas flow in a finite porous bed. *Trans. ASME*: *J. Fluids Engng* **12**, 779–781.

Nishida, M. 2001 Shock Tubes. In *Handbook of Shock Waves* (ed. G. Ben-Dor, O. Igra & T. Elperin), vol. 1, pp. 553–585. Academic.

Rogg, B., Hermann, D. & Adomeit, G. 1985 Shock induced flow in regular arrays of cylinders and packed beds. *Intl J. Heat Mass Transfer* **28**, 2285–2287.

Sakakita, H. & Hayashi, K. 1992 Study on pressure profiles in a powder layer using a vertical shock tube. In *Proc. Natl Symp. On Shock Waves 92, Japan*, pp. 655–660.

Sen, S., Mohan, T. R. K., Visco, D. P., Swaminathan, S., Sokolow, A., Avanos, E. & Nakagawa, M. 2005 Using mechanical energy as a probe for the detection and imaging of shallow buried inclusions in dry granular beds. *Intl J. Mod. Phys.* **B19**(18), 2951–2974.

Smeulders, D. M. J., van Dongen, M. E. H. & Wisse, C. J. 1997 Acoustic slow wave transition in air-saturated porous media. *Proc. 21st Intl Symp. Shock Waves, Great Keppel Island, Australia*, Paper 6911.

Sodre, J. & Parise, J. 1998 Fluid flow pressure drop through an annular bed of spheres with wall effects. *Expl Thermal Fluid Sci.* **17**, 265–275.